

# Chapter 4

## Magnetic Properties in Nondestructive Testing

It has been known for many years that the magnetic properties of steels depend on their composition and heat treatment. Mechanically harder steels have superior properties as permanent magnets than softer steels, hence the terminology of ‘hard’ and ‘soft’ magnetic materials. Curie (1898) found a relationship between magnetic behaviour and carbon content in permanent magnet steels, and Evershed (1925) observed a deterioration of magnet steel properties over time, which he related to slow metallurgical changes. Such relationships suggested that magnetic measurements could be used as a nondestructive testing (NDT) method to determine materials properties. In recent decades, many investigations have been carried out to develop such techniques; progress has been reviewed by Blitz (1991), Swartzendruber (1992), Devine (1992), Sipahi (1994), Sablik and Augustyniak (1999) and Ara (2002).

### 4.1 Hysteresis properties

#### 4.1.1 The hysteresis loop

Figure 4.1 is a plot of magnetisation  $M$  against applied field  $H$ . On application of a field to a demagnetised sample,  $M$  increases with  $H$ , reaching the saturation magnetisation  $M_S$  if a sufficiently large field is applied. When  $H$  is reduced, and subsequently cycled between positive and negative directions,

$M$  follows a hysteresis loop. A *major loop* (solid line) is one in which the saturation magnetisation  $M_S$  of the material is reached; if this is not the case, the curve is a *minor loop* (dashed line). The parameters most commonly used to characterise hysteresis are the field  $H_C$  required to reduce  $M$  to zero, the value  $M_R$  of  $M$  when  $H = 0$ , and the hysteresis energy loss  $W_H$ , which is determined from the area enclosed by the loop.  $H_{\max}$  is the maximum applied field and  $H_S$  the field at which  $M = M_S$ .

The positions of greatest slope change are known as ‘knees’; one of these is marked on Figure 4.1. The slope  $dM/dH$  of the initial magnetisation curve at  $(H = 0, M = 0)$  is the initial differential susceptibility  $\chi'_{\text{in}}$ , and that of the hysteresis loop at  $H = H_C$  is the maximum differential susceptibility  $\chi'_{\text{max}}$ . The terminology ‘square’ and ‘sheared’ is used to describe loops with large and small values of  $\chi'_{\text{max}}$  respectively. The hysteresis parameters are in general regarded as independent, but in some materials, linear relationships have been found between, for example,  $W_H$  and  $H_C$  (Jiles, 1988a, b).

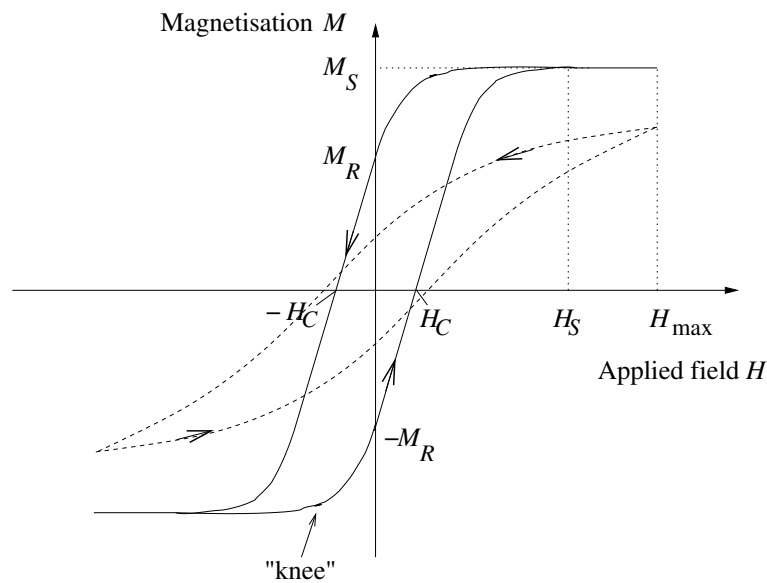


Figure 4.1: A major hysteresis loop (solid line), showing the coercive field  $H_C$ , remanence  $M_R$  and saturation magnetisation  $M_S$ , and a minor loop (dashed line). The arrows show the direction of magnetisation.

### 4.1.2 Alternative terminology

The magnetic induction  $\mathbf{B} = \mu_0(\mathbf{H} + \mathbf{M})$  is sometimes used instead of  $\mathbf{M}$ .  $B$ - $H$  and  $M$ - $H$  loops contain the same information but different terminology is used:  $B_S$  and  $B_R$  instead of  $M_S$  and  $M_R$ , respectively. The slope of a  $B$ - $H$  loop,  $dB/dH$ , is the differential permeability,  $\mu'$ ; the maximum value of this usually occurs at  $H = H_C$  and is denoted  $\mu'_{\max}$ . The magnetic flux  $\Phi$  is the product of  $\mathbf{B}$  and the sample cross-sectional area.

$H_C$  is usually referred to as the coercive field, and  $B_R$  and  $M_R$  as the remanent induction and remanent magnetisation respectively. The alternative terms ‘coercivity’ and ‘remanence’ are also used, but an emerging convention (noted by Jiles, 1998) is to reserve these last two terms for major loops only<sup>1</sup>.

Hysteresis experiments for use in NDT usually involve measurement of the  $M - H$  or  $B - H$  loop and extraction of a selection of the above parameters. An alternative approach, developed by Davis (1971) and Willcock and Tanner (1983a, b), is to express the loop in terms of Fourier coefficients. This method is used in industry for stress monitoring using magnetic hysteresis (Tanner, personal communication), and has the advantage that the entire data set is used, but it has not so far been adopted for microstructure-based investigations.

## 4.2 Magnetic noise

### 4.2.1 Barkhausen effect

Barkhausen (1919) discovered that, during the magnetisation of an iron bar, many short-lived voltage pulses were induced in a coil wound around the bar. These were detected as audible clicks in a loudspeaker. By electromagnetic induction, the voltage depends on the rate of change of magnetisation with time; discrete pulses imply abrupt changes in magnetisation. Even when care was taken to change the magnetising field smoothly, the discontinuities persisted, demonstrating that magnetisation was an intrinsically discrete pro-

<sup>1</sup>A distinction also exists between the *coercivity*, at which  $B = 0$ , and the *intrinsic coercivity*, at which  $M = 0$ , but this can be neglected for steels, in which  $H_C$  is small.

cess. Barkhausen used this observation to support the hypothesis of magnetic domains predicted theoretically by Weiss (1906, 1907). The characteristics of the Barkhausen noise (BN) signal depend on several factors, including microstructure.

### 4.2.2 Magnetoacoustic effect

The abrupt motion of Type-I domain walls is accompanied by a change in the magnetostrictive strain. This causes an acoustic wave, which travels through the material and can be picked up on the surface by a piezoelectric transducer (Lord, 1975). Since such magnetoacoustic emission (MAE) arises only from Type-I wall motion, but BN can be produced by any sudden change in the magnetisation state, measuring both properties gives complementary information.

### 4.2.3 Magnetic noise measurement

The basis of a BN measurement system is an electromagnetic yoke to produce an alternating field and a pickup coil to detect the noise pulses, but two variations exist. The sample may be positioned within the yoke, with the pickup coil surrounding the sample (Figure 4.2 (a)). This restricts the sample size and shape, and is therefore inconvenient for NDT. The alternative method uses a yoke placed onto a flat sample, and a pickup coil on or near the surface (Figure 4.2 (b)). MAE measurements are made using an arrangement similar to (b), but with a piezoelectric transducer bonded directly to the sample surface instead of a pickup coil.

Comparisons of magnetic noise literature reveal considerable differences in yoke geometry, experimental conditions and signal processing. In some cases, the influences of these factors on the signal have been investigated (§ 4.9), but such characterisations are not comprehensive.

### 4.2.4 Data analysis

The raw magnetic noise data are a series of voltage pulses, and their associated applied field values, obtained as a function of time (Figure 4.3 (a)).

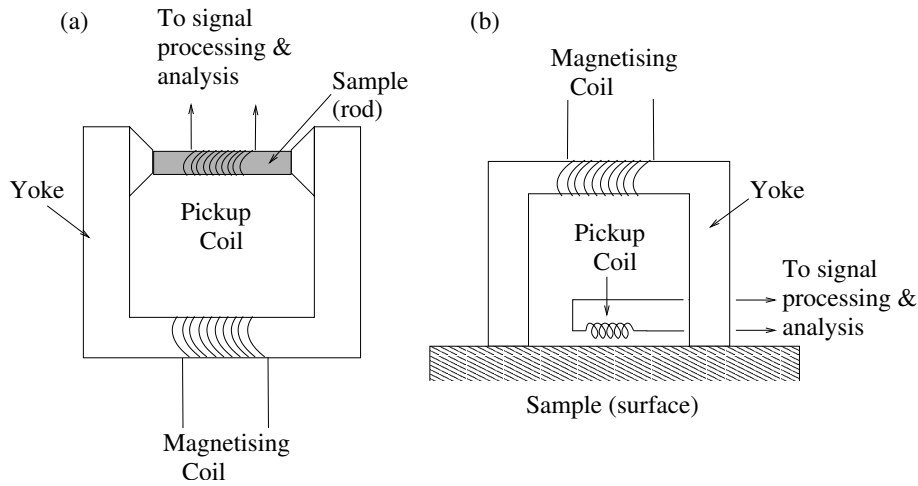


Figure 4.2: Typical measurement apparatus for magnetic noise: (a) magnetising yoke with rod-shaped specimen, (b) surface sensor.

The noise signal consists of a stochastic component superposed on a smooth variation with applied field. To obtain this variation, the root-mean-square (RMS) of the noise over several field cycles is obtained; a smoothing algorithm may also be applied. Figure 4.3 (b) shows the RMS noise in the increasing-field direction (solid line) and in the opposite direction (dotted line). These two curves are usually mirror images in  $H = 0$ , so only one direction is displayed. All subsequent diagrams and discussions will use increasing-field curves unless otherwise stated.

Fourier analysis can be used to study the noise frequency content (c). The square of the voltage is often referred to in the literature as the ‘noise power’, and a plot such as (c) as a frequency spectrum. Other plots frequently encountered in the literature are the size distribution of noise pulses (‘pulse height distribution, PHD’ (d)) and the number of pulses versus time or applied field (not shown, but of similar form to (b)). In addition, single parameters have been used to characterise the noise signal: the maximum pulse size, RMS pulse size, total number of pulses and the noise energy, calculated as the integral of the RMS noise signal over a whole cycle.

The large number of characterisation methods can lead to some difficulty in comparing the results of investigations, since the same quantities are not

always measured.

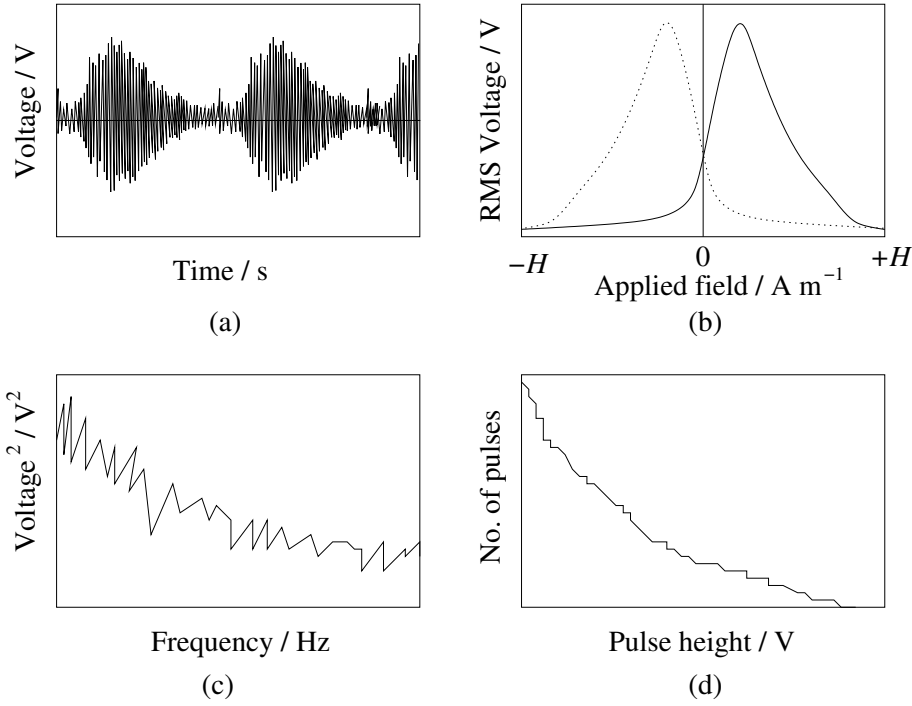


Figure 4.3: Magnetic noise plots: (a) Raw noise versus time. (b) Root-mean-square (RMS) noise versus applied field. (c) Noise voltage versus frequency (Fourier transform). (d) Pulse height distribution plot.

## 4.3 Applications of magnetic NDT

### 4.3.1 Microstructural type determination

Martensitic steels consistently have the greatest  $H_C$ , and ferrite-pearlite microstructures the least, with bainitic steels intermediate between these extremes (Jiles, 1988b; Mitra *et al.*, 1995, Saquet *et al.*, 1999). This should allow identification of the basic microstructural state with a simple magnetic measurement. BN measurements have also been used successfully to differentiate between microstructural states across the heat-affected zone of a weld (Moorthy *et al.*, 1997a).

### 4.3.2 Empirical correlations

Correlations for the determination of mechanical or microstructural properties using magnetic measurements have been found in many materials. Examples include extensive work in the former Soviet Union on monitoring the quality of heat-treatment and hardening in a variety of steels (Mikheev *et al.*, 1978; Kuznetsov *et al.*, 1982, Zatsepin *et al.*, 1983; Mikheev, 1983). Devine (1992) describes many more such results.

The important consideration for NDT is that there is a monotonic change in the magnetic property within the range of interest, as pointed out by Halmshaw (1991). Correlations are specific to particular microstructures and ranges of composition and temperature, and are liable to fail outside these limits. For example, in a pearlitic rail steel, the correlation between coercive field and hardness was poor at room temperature, but good at high temperatures (Bussière *et al.*, 1987). The suggested reason for this was that at high temperatures, the  $\text{Fe}_3\text{C}$  particles were above their Curie temperature  $T_C$ , and so acted as nonferromagnetic inhomogeneities.

Findings such as these have led to investigations of the effects of individual microstructural features, such as grain boundaries, dislocations and inclusions, on the magnetic properties.

## 4.4 Grain boundaries

### 4.4.1 Grain size effects

#### High-purity materials

Two distinct theoretical models predict that  $H_C$  should be proportional to  $1/d$ , where  $d$  is the average grain diameter, in materials where grain boundaries are the dominant obstacle to domain wall motion (Goodenough, 1954; Globus and Guyot, 1972). Degauque *et al.* (1982) found that this relationship was valid for annealed high-purity iron, although  $d^{-1/2}$  also fitted the data satisfactorily. In commercial-purity nickel, too, the coercive field decreased with increasing grain size over a wide range from nanocrystalline to  $\sim 10^2 \mu\text{m}$  (Kawahara *et al.*, 2002).

The total number of pulses of both BN and MAE decreased with increasing grain size in nickel, following a  $1/d$  dependence (Ranjan *et al.*, 1986, 1987a). In pure nickel, the RMS BN voltage was a minimum at an intermediate value of  $d$  (Hill *et al.*, 1991); an examination of the variation of noise voltage with applied field showed that the peak heights and positions changed with grain size in a complex way. It appears that using a single parameter to characterise the noise voltage is too simplistic in nickel. In pure iron, the RMS noise amplitude scaled with  $d^{-1/2}$  (Yamaura *et al.*, 2001).

These results are collated in Table 4.1. The occurrence of both  $d^{-1}$  and  $d^{-1/2}$  relationships may be due to experimental uncertainty allowing both to fit adequately (Degauque *et al.*, 1982). Since a  $d^{-1}$  relationship was predicted theoretically, this may have been the only fit attempted in some cases. Also, it has not been established theoretically that all the properties measured should depend on grain size in the same way. Further work on the interdependence of these properties would be useful.

Property	Pure Fe	Pure Ni	Mild steels
Coercive field	$\downarrow^D (\propto d^{-1}, d^{-1/2})$	$\downarrow^K$	$\uparrow^R, \downarrow^{Yo}$
BN:			
Total counts		$\downarrow^R (\propto d^{-1})$	$\uparrow^R$
RMS voltage		$\downarrow(\text{small } d) \uparrow(\text{large } d)^H$	$\uparrow(\propto d)^R$
Max. voltage			$\downarrow^A$
Peak height			$\downarrow^{S,G}$
$H$ of peak			$\downarrow^G$
Integrated	$\downarrow^{Ya} (\propto d^{-1/2})$		
MAE:			
Total counts		$\downarrow^R (\propto d^{-1})$	$\uparrow^R$
RMS voltage			$\uparrow^R(\propto d)$

Table 4.1: Variation of magnetic properties with increasing grain size: (A)nglada-Rivera *et al.*, 2001, (D)egauque *et al.*, 1982, (G)atelier-Roth ea *et al.*, 1992, (H)ill *et al.*, 1991 (K)awahara *et al.*, 2002, (R)anjan *et al.*, 1986, 1987a, b, (S)hibata and Sasaki, 1987, (Ya)maura *et al.*, 2001 (Yo)shino *et al.*, 1996.

### Mild steels

The final column of Table 4.1 displays results from mild steels. In decarburised steel, all the properties show opposite trends to those in the purer metals; for example, the RMS noise voltages are directly proportional to  $d$  (Ranjan *et al.*, 1986, 1987a). This was explained by the presence of impurities – MnS particles within the grains and phosphorus on the grain boundaries – whose presence overwhelmed the intrinsic grain size effect (Ranjan *et al.*, 1987b). However, Yoshino *et al.* (1996) reported that in steels containing only ferrite,  $H_C$  was inversely proportional to the grain size.

The average BN amplitude in low carbon steel (composition not specified) varied as  $\ln d/d_C$ , where  $d_C$  is the extrapolated grain size for which the BN amplitude is zero, for small grain size  $d$ , and saturated at a critical value of  $d$  (Tiitto, 1978).

The variation of BN and MAE voltage with position in the magnetisation cycle for 0.1 wt. % C steel showed two peaks (Shibata and Sasaki, 1987). For BN, the first of these decreased in height with increasing grain size, while the second showed little variation. The first MAE peak occurred at a stronger applied field than the first BN peak, but the second peaks coincided. It was concluded that the first peak was due to domain wall motion, which occurred at a lower field for Type-II than for Type-I walls, while the second peak was attributed to discontinuous rotation of domains.

In Fe-0.013 wt. % C, a single BN peak, whose height decreased with increasing grain size, was seen (Gatelier-Roth ea *et al.*, 1992). Similarly, in 0.4 wt. % C steel, the maximum BN amplitude was largest in a fine-grained and smallest in a coarse-grained sample (Anglada-Rivera *et al.*, 2001). In both cases, these results were explained as due to a larger number of domain walls within fine-grained samples. The domain size was reported by Degauque *et al.* (1982) as proportional to the square root of grain size for grain diameters between 0.05 and 10 mm. Hence, both the the number of domain walls and the number of pinning sites per unit volume is greatest for small grains.

The BN peaks observed by Gatelier-Roth ea *et al.* (1992) were situated

just beyond  $H = 0$ . They moved closer to  $H = 0$ , corresponding to a decrease in pinning strength, with increasing grain size.

### Complex microstructures

In the equiaxed, single-phase materials discussed above, grain boundaries are the only important microstructural feature. For NDT of more complex microstructures, the relative influence of grain boundaries and other features must be determined.

In pearlitic plain-carbon steels with a variety of carbon contents and fabrication histories, a linear trend was observed between  $H_C$  and  $d^{-1}$ , but the fit was not particularly good (Tanner *et al.*, 1988). However, much better agreement was obtained using the equation:

$$H_C = (c_1 V_P / d_P) + (c_2 V_F / d_F) \quad (4.1)$$

where  $V_P$  and  $V_F$  are the pearlite and ferrite volume fractions, and  $d_P$  and  $d_F$  the pearlite and ferrite grain sizes, respectively;  $c_1$  and  $c_2$  are constants.

Yoshino *et al.* (1996) found that the presence of pearlite did not significantly affect  $H_C$  at phase fractions  $< 0.17$ . When pearlite constituted more than 0.6 of the microstructure,  $H_C$  increased in proportion to the pearlite fraction and was no longer affected by the grain size. Similarly, in ferritic steels containing  $> 0.15$  martensite,  $H_C$  was dominated by the martensite fraction rather than the ferrite grain size.

In austenitised, quenched and tempered plain-carbon and 12 wt. % Cr steel, the prior austenite grain size had a negligible effect on the hysteresis loop characteristics, which depended instead on hardness (Kwun and Burkhardt, 1987). It is clear that the formation of martensitic or bainitic microstructure, and the changes accompanying tempering, are the governing processes in quenched and tempered steels.

#### 4.4.2 Grain boundary misorientation

In coarse-grained Fe-3 wt. % Si, the BN signal was measured on individual grain boundaries and within the grains adjacent to them (Yamaura *et al.*,

2001). The relative BN intensity at the boundary,  $R_{\text{intensity}}$ , was calculated from:

$$R_{\text{intensity}} = \frac{P_{\text{GB}} - P_{\text{AVG}}}{P_{\text{AVG}}} \quad (4.2)$$

where  $P_{\text{GB}}$  and  $P_{\text{AVG}}$  are the noise power on the grain boundary and the average of the noise powers from the adjacent grains respectively. The increase of  $R_{\text{intensity}}$  with boundary misorientation angle is shown in Figure 4.4. Only low-angle boundaries were found in the material.

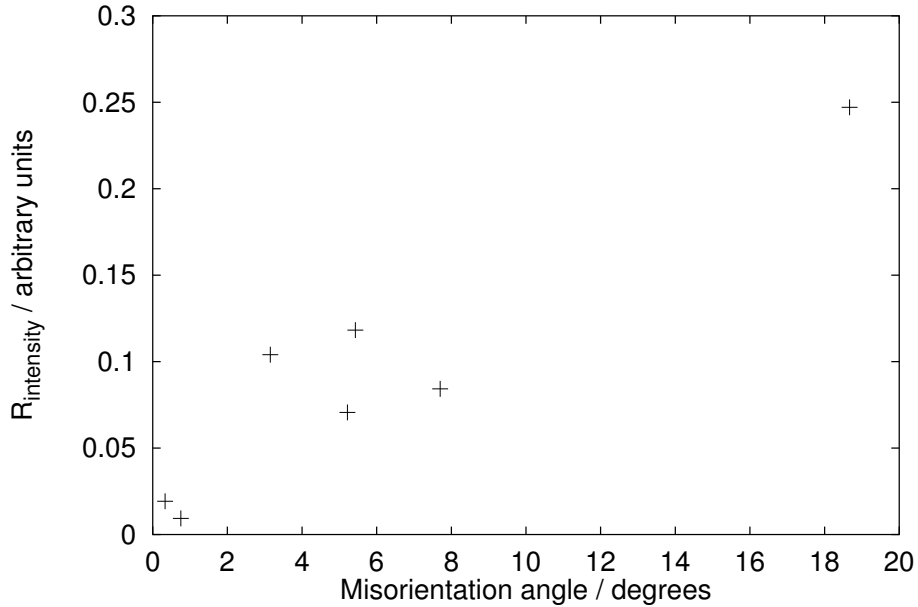


Figure 4.4: Dependence of  $R_{\text{intensity}}$  on misorientation angle in Fe-3 wt. % Si (Yamaura *et al.*, 2001).

### 4.4.3 Grain size influence on BN frequency

In pure iron, the ratio of high-frequency to low-frequency components of the BN signal decreased as the grain size increased (Yamaura *et al.*, 2001). This was quantified using the parameter  $P_{60}/P_3$ , where  $P_{60}$  is the total noise with frequency 60 kHz and  $P_3$  the noise with frequency 3 kHz; its variation with grain size is shown in Figure 4.5. The high-frequency noise was attributed

to emissions from defects such as dislocations and grain boundaries, which become less important as coarsening occurs, resulting in a decrease in  $P_{60}/P_3$  (Yamaura *et al.*, 2001). Another interpretation is that the noise frequency is approximately the reciprocal of the time taken by a domain wall to move from one pinning site to the next, and this in turn is proportional to the distance between obstacles (Saquet *et al.*, 1999). Hence, in coarser microstructures, the proportion of high-frequency noise is lower.

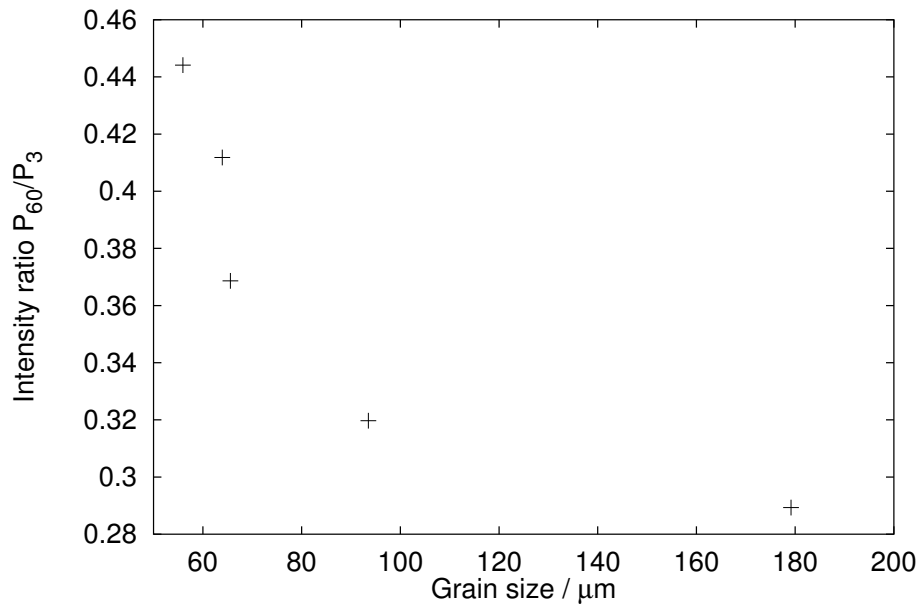


Figure 4.5: Relationship between frequency components of BN and grain size (Yamaura *et al.*, 2001).

#### 4.4.4 Summary

In pure materials, relationships between grain size and magnetic properties are mostly simple, with decreases in coercive field and the level of BN and MAE as grain size increases. In mild steels, some inconsistencies have been found, but the general trend is also towards lower values of most properties as grain size increases. The opposing trends in peak height and average event size are not irreconcilable, since the noise peak height depends on both the number of events, which is smaller when there are fewer pinning sites and

moving walls, and the average event size, which is large when a domain wall can move a long distance without being pinned.

The pinning strength of grain boundaries was slightly greater for smaller grains. Finer-grained iron also gave a greater proportion of high-frequency noise; this can be related to a shorter domain wall time-of-flight between obstacles. At individual low-angle grain boundaries in Fe-3 wt. % Si, the ratio of the noise measured across the boundary to the noise from the adjacent grains increased with misorientation angle.

In steels with a second microstructural constituent, this tended to dominate magnetic behaviour when it was present in sufficient quantities. Similarly, in austenitised, quenched and tempered steels, the prior austenite grain size had no significant effect on hysteresis properties.

## 4.5 Dislocations and plastic strain

### 4.5.1 Deformation

At a low level of deformation in pure iron, isolated, homogeneously distributed dislocations appeared, but caused very little change in  $H_C$  compared to the undeformed state (Astié *et al.*, 1981). Further deformation produced dislocation tangles and a rapid increase in  $H_C$  with stress. At even higher strain, dislocations formed subgrain boundaries and the intragranular dislocation density decreased.  $H_C$  still increased with stress, but the rate of increase was smaller.

Jiles (1998b) investigated the effect of plastic compressive deformation on a high-chromium steel in three microstructural conditions: ferrite/pearlite, ferrite/bainite and tempered martensite. The coercive field was proportional to the hardness irrespective of the microstructure. However, some microstructural differences were evident. In ferrite/pearlite and ferrite/bainite,  $W_H$  and  $H_C$  increased with increasing plastic strain; this was attributed to the additional obstacles to domain wall motion provided by a greater dislocation density. In martensite, by contrast,  $H_C$  and  $W_H$  decreased with increasing plastic strain. It was suggested that this, in the same way as the

observations of Astié *et al.* (1981), was due to the formation of subgrains, between which the dislocation density would be relatively low.

### 4.5.2 Annealing of deformed materials

Previously deformed specimens of pure nickel were annealed at various temperatures, and the hardness and total BN and MAE counts determined (Ranjan *et al.*, 1987c; Figure 4.6). The hysteresis loss and MAE count number depended on temperature in the same way as the hardness, but the BN behaviour was more complex. It was suggested that this was due to a competition between the reduction in dislocation density, which reduces the number of domain wall pinning sites, and the nucleation of small recrystallised grains, which increases it. The lack of a similar trough in the MAE counts at 400°C was attributed to a smaller effect of grain size on MAE than on BN.

Plots of BN and MAE versus applied field both showed single peaks in deformed nickel. Prolonged annealing reduced the peak height by about 80%, demonstrating that it was due to pinning by dislocations (Buttle *et al.*, 1987a).

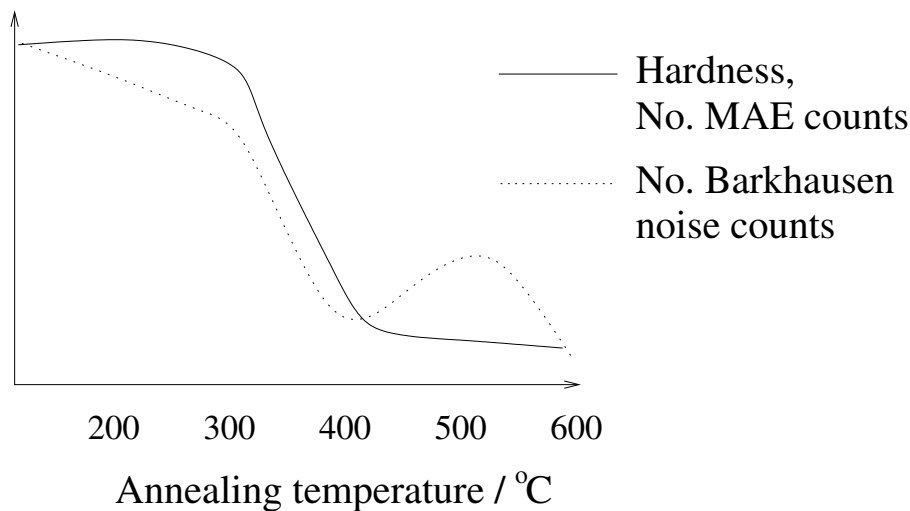


Figure 4.6: Effect of annealing temperature on mechanical and magnetic properties of deformed nickel (Ranjan *et al.*, 1987c).

Similarly, the BN and MAE properties of pure iron, plastically deformed

then annealed for 1 hour at a range of temperatures, were investigated (Buttle *et al.*, 1987a). The total event count and maximum event size for both BN and MAE depended on annealing temperature in a similar way to the MAE total count in nickel shown in Figure 4.6, but with a slight increase before the abrupt drop. The ‘trough’ observed by Ranjan *et al.* (1987c) in nickel was absent in iron.

Figure 4.7 shows the variation of BN and MAE voltage with applied field for a sample annealed below 550°C. The outer peaks of the BN signals, and the two peaks in the MAE, correspond to the ‘knees’ of the hysteresis loop. Up to 550°C, the BN peak at the negative knee grew, the central peak decreased slightly in height, and the two MAE peaks both grew, with increasing temperature. Above 550°C, all the peaks decreased rapidly to almost nothing.

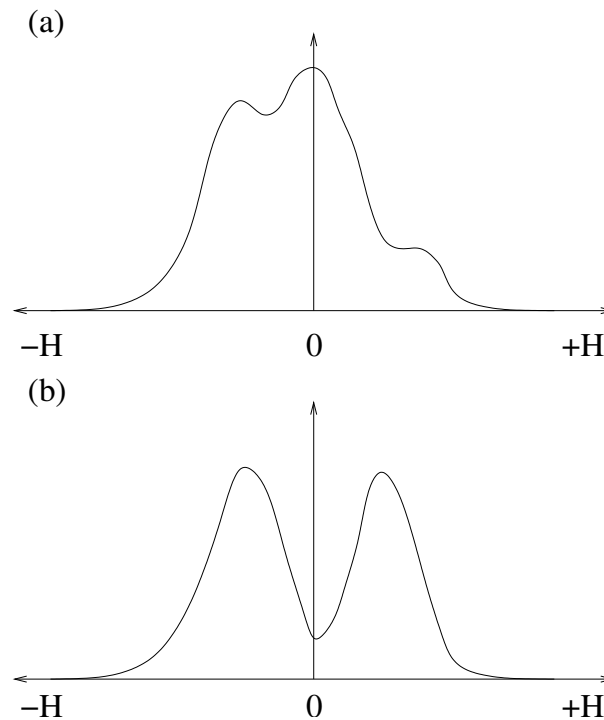


Figure 4.7: (a) BN signal from pure iron, cold-worked and annealed below 550°C; (b) MAE signal from the same sample (Buttle *et al.*, 1987a).

The BN and MAE peaks situated at the negative knee were attributed

to domain nucleation, and those at the positive knee to domain wall annihilation. The former are higher because a larger energy is required to nucleate domains, resulting in a smaller number of large-amplitude events. Annihilation, by contrast, may involve the sweeping out of only small volumes at a time, and hence the individual pulses need not be large. However, this argument makes the assumption that the peak height will be greater for a small number of large events than for a large number of small ones. It is not obvious whether this is indeed the case.

The BN peak close to  $H = 0$  had no MAE equivalent. Since only Type-I domain wall motion produces MAE, Buttle *et al.* concluded only Type-II wall activity was occurring in this region. This behaviour was believed to be in agreement with the prediction of Scherpereel *et al.* (1970) that dislocations should interact more strongly with Type-II than with Type-I walls.

However, a more simple explanation could be that the difference in BN and MAE activity around  $H = 0$  is related to the smaller number of Type-I walls present. A magnetoelastic energy penalty is involved in creating a domain at  $90^\circ$  to another (§ 3.1.3), so the preferred domain structure contains predominantly parallel, Type-II walls, with Type-I walls appearing only to provide flux closure at magnetic inhomogeneities. Secondly, if Type-II walls undergo stronger interactions with dislocations than do Type-I walls, the peak for the Type-II interaction should appear at a higher applied field than that for the Type-I, but there does not seem to be any evidence of this.

### 4.5.3 Deformation and saturation effects

Figure 4.8 shows the effect of deformation on the BN and hysteresis behaviour of a mild steel (Kim *et al.*, 1992). In the annealed, unstrained state, the hysteresis loop has straight, steep sides, and magnetisation change takes place over a small range of field. BN peaks are present at the knees. Straining causes a change to a sheared loop with a smaller saturation value, and a single, central BN peak coinciding with the peak in  $dB/dt$ .

Kim *et al.* also found that reducing  $H_{\max}$  decreased the outer BN peak heights and increased the conformity between the BN curve and  $dB/dt$  (Fig-

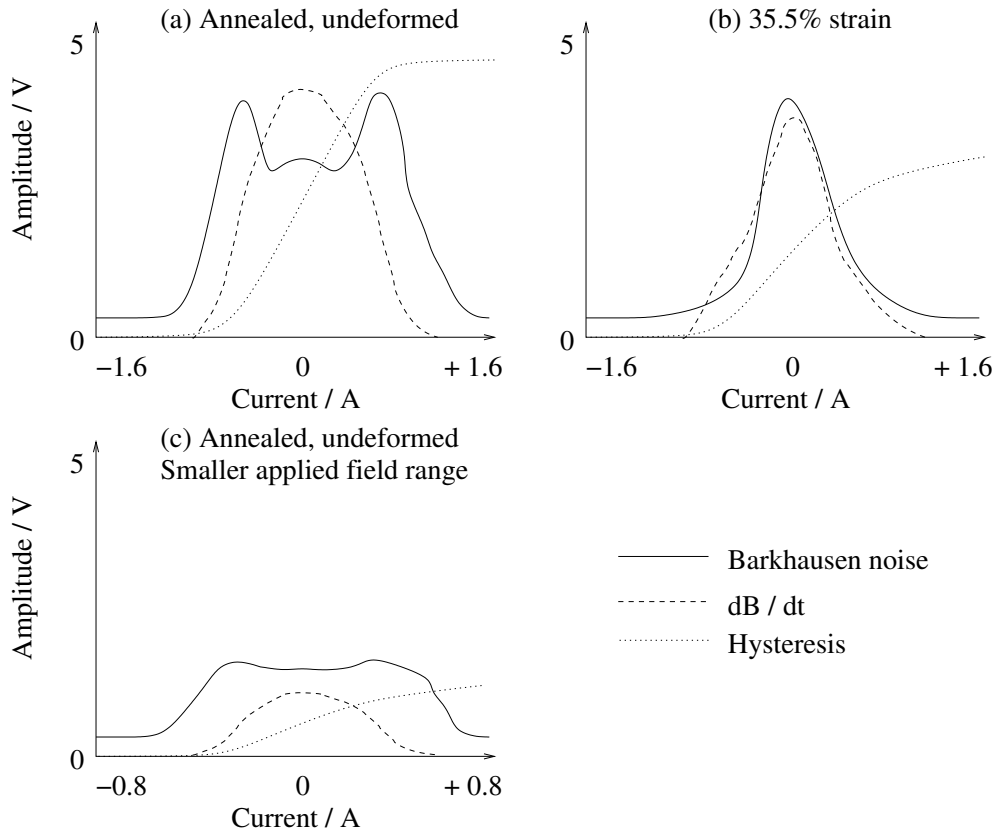


Figure 4.8: Effect of straining and changing the applied current range (and hence  $H_{\max}$ ) on BN, hysteresis and  $dB/dt$  curves (Kim *et al.*, 1992).

ure 4.8 (c)). The ability of both deformation and reduction of  $H_{\max}$  to suppress the outer peaks led to the conclusion that domain nucleation and annihilation did not take place in many of the domains in the deformed material. The dramatic reduction in the value of  $M$  at  $H_{\max}$  supports this; it is unlikely that the true  $M_S$  (which is generally viewed as a structure-insensitive property) could be changed to this extent by deformation. Instead, it seems that the highly dislocated material does not become fully saturated. The BN activity around zero field increases on deformation. It appears that in a relatively strain-free sample, it is easy for the structure to ‘switch’ from one state of near-saturation to another, but when many dislocations are present, domain walls must overcome these, with an associated emission of BN around

$H = 0$ .

#### 4.5.4 Summary

In many cases, there is a simple linear correlation between hardness and  $H_C$ , but when the dislocation density is very high, this relationship is altered by the formation of subgrain boundaries.

In pure iron and nickel, magnetic noise levels are high after deformation, but decrease to almost nothing after high-temperature annealing. By contrast, in mild steel, the large BN signal from annealed material was reduced by deformation. This was accompanied by a change from three peaks to only one. The outer peaks have been attributed to domain nucleation and annihilation and the central region to pinned domain wall motion. Heavy deformation increases the number of pinning sites and increases the difficulty of saturation so that the outer two peaks disappear.

## 4.6 Second-phase particles

### 4.6.1 Ideal systems

The study of particle effects on magnetic properties in steels is complicated by the inhomogeneous distribution of some precipitates, which nucleate preferentially on grain boundaries (§ 2.3.4) and by the ferromagnetic nature of  $\text{Fe}_3\text{C}$  and some other carbides below their Curie temperatures. To determine the essential features of particle effects, ‘ideal’ systems, which avoid these complexities, have been studied.

Magnetic precipitation hardening is an increase in  $H_C$  due to the formation of a precipitate phase on ageing. Shilling and Soffa (1978) found that this effect was linked to a periodic array of fine particles coherent with the matrix. Within this regime,  $H_C$  could be increased by increasing the volume fraction or size of particles. Overageing, *i.e.* reduction in  $H_C$ , was associated with a loss of periodicity. In the periodic alloy, the Kersten pinning theory (§ 3.3.1) was adequate for describing changes in  $H_C$ .

‘Incoloy 904’ nickel-based superalloy (33.8 Ni, 51.0 Fe, 14.0 Co,

1.2 Ti wt. %) was selected as an ideal system because the second phase is nonferromagnetic, nucleates homogeneously, is distributed evenly in the matrix and grows as spheres on ageing (Buttle *et al.*, 1987b). A monotonic increase in  $H_C$  with ageing time was observed, but the total BN event count showed a maximum at an intermediate time.

Domain wall-particle interactions were observed using Fresnel and Foucault microscopy (§ 3.4). Small particles deflected the walls slightly. As the applied field was increased, small wall displacements occurred in a quasi-continuous manner, passing through several inclusions at a time, up to a critical field at which a long-range domain wall jump occurred. When the particles were large, domain wall motion occurred in discrete jumps. The inclusions were surrounded by closure domains, which grew as the particles coarsened, to form an interacting network. This limited the domain wall jump size, since the wall was pinned by the networks rather than individual particles.

The maximum Barkhausen event size increased with ageing time in single-crystal Incoloy 904, but remained approximately constant in polycrystalline samples. This was attributed to the limitation of jump distances by grain boundaries. The maximum volume swept out in a single jump was calculated using BN data and found to be of similar magnitude to the grain size as observed by scanning electron microscopy.

As in the dislocation study (Buttle *et al.*, 1987a; § 4.5.2) the BN and MAE profiles both had peaks at the hysteresis loop knees, and an additional central peak was present in the BN signal. The BN peak heights increased up to an annealing time of 520 h, at which stage the inclusion diameter was about the same as the wall width, then decreased again after longer annealing. Buttle *et al.* (1987b) again attributed the outer peaks to domain nucleation and annihilation, and the central peak to domain wall motion, predominantly of Type-II walls. Very little noise activity occurred around  $H = 0$  in unaged specimens; this was explained by the ease of domain wall motion in a matrix with few pinning points.

Buttle *et al.* suggested that the closure domains on large inclusions may persist at high fields, and regrow when the field is reduced, avoiding the

necessity for additional nucleation. This may explain why the outer BN peaks decrease in height after long ageing times.

#### 4.6.2 Effect of carbon on hysteresis properties

On the basis of the Néel theory (§ 3.3.1), a maximum in  $H_C$  was predicted at the Curie temperature of  $\text{Fe}_3\text{C}$  in plain-carbon steels (Figure 4.9). This was sought unsuccessfully by Dijkstra and Wert (1950) and others, so it was concluded that  $\text{Fe}_3\text{C}$  behaved ‘as if nonmagnetic’. However, English (1967) found such maxima in pearlitic Fe-0.8 wt. % C and 2Cr-1C wt. % steel. The temperatures at which they occurred were different for the two steels, and this was attributed to the modification of the carbide composition, and therefore its magnetic behaviour, by the presence of chromium in the carbide.

In coarse spheroidised pearlitic microstructures, no  $H_C$  anomaly was found. English suggested that this may have been due to interparticle interactions, such as the formation of a network of spike domains, which did not allow the particles to be considered in isolation.

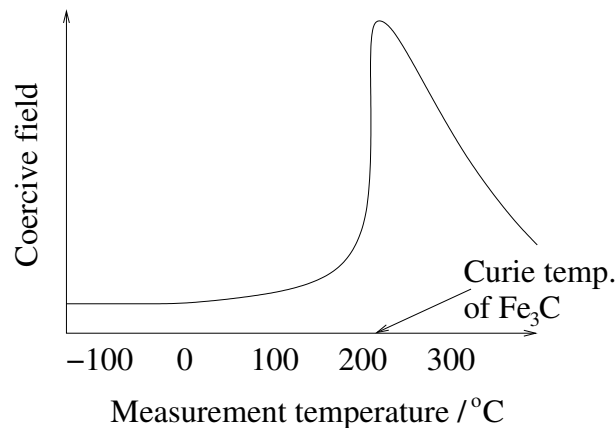


Figure 4.9: Anomaly in the coercive field predicted at the Curie temperature of  $\text{Fe}_3\text{C}$  (English, 1967).

In plain-carbon steels,  $H_C$  increased with carbon content in both pearlitic and spheroidal microstructures; this was a much stronger influence on  $H_C$  than that of grain size (Ranjan *et al.*, 1986, 1987; Jiles, 1988a). Monotonic

increases in  $H_C$  and  $W_H$  were observed for both microstructures, but the values of these properties were always higher in the pearlitic steels (Jiles, 1988a; Figure 4.10). This result was later confirmed by Lo *et al.* (1997b). The remanent magnetisation was independent of the carbon content, but affected by the carbide morphology, being higher in the spheroidal microstructures (Jiles, 1988a).  $H_C$  increased with hardness, irrespective of the microstructure (Jiles, 1988a; Tanner *et al.*, 1988) and varied linearly with the volume fraction of carbide (Jiles, 1988a). In this case, the proportionality constant depended on the carbide morphology. In addition,  $H_C$  depended on the volume fraction of pearlite grains.

Spike domains were again believed to be responsible for the difference in properties between spheroidal and lamellar structures, but in this case it was considered that the spikes on spheroids weakened domain wall-particle interactions compared to those in pearlite.

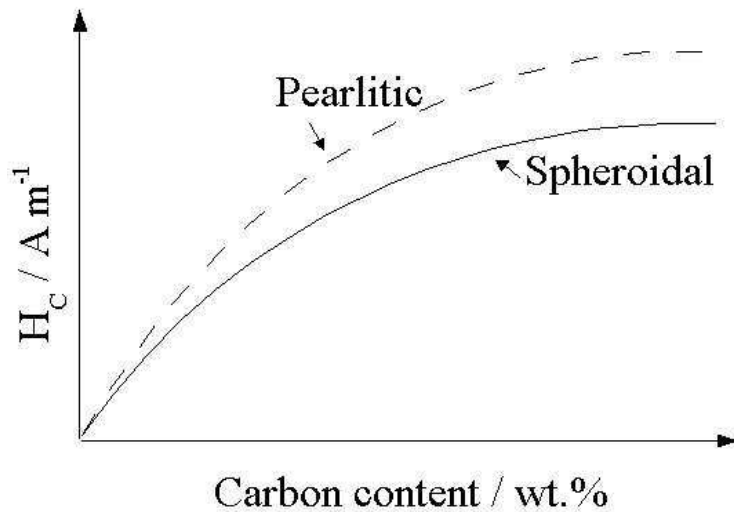


Figure 4.10: The effect of carbon content on coercive field in plain-carbon steel, for spheroidal and pearlitic microstructures (Jiles, 1988a).

Tanner *et al.* (1988) found that  $H_C$  increased with increasing carbon content in steels in which only the carbon content varied, but this relationship broke down in C-Mn steels. However,  $H_C$  was related to a weighted sum of carbon and manganese contributions:

$$H_C = 1.186(\text{ wt. \% C}) + 0.237(\text{ wt. \% Mn}) \quad (4.3)$$

This relationship is not general; in particular, it did not correctly predict  $H_C$  for manganese-free steels.

Fe-C alloys were prepared with carbon in solution (State A), as  $\sim 0.5 \mu\text{m}$  intragranular precipitates (B), and as larger carbides ( $\sim 10 \mu\text{m}$ ) at grain boundaries (C) to compare their hysteresis properties (Lopez *et al.*, 1985). In C, islands of pearlite were also present when the carbon content was over 0.02 wt. %.  $H_C$  increased with increasing carbon content in all cases, but was much greater in State B samples (Figure 4.11). Plots of  $W_H$  and remanence against carbon content were similar to Figure 4.11. The interstitials in A, while exerting a dragging force, did not have a strong effect on large domain wall displacements. Grain-boundary precipitates, because of their wide spacing, also only weakly affected  $H_C$ . Fine particles, whose diameters were twice or three times the wall thickness, interacted strongly with domain walls. The carbon contents in this investigation were small (0.01–0.05 wt. %) so it is unlikely that closure domain networks were formed.

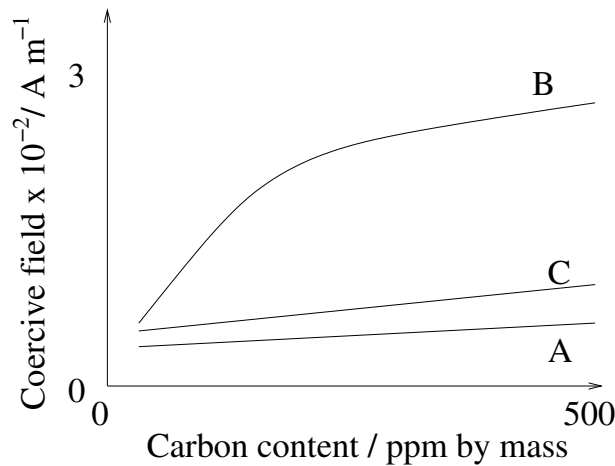


Figure 4.11: The effects of different precipitation states on the coercive field (A) carbon mostly in interstitial solution, (B) intragranular precipitates of around  $0.5 \mu\text{m}$  diameter, (C) large carbides of around  $10 \mu\text{m}$  diameter at grain boundaries (Lopez *et al.*, 1985).

### 4.6.3 Effect of carbon on BN and MAE

A single, very sharp RMS BN peak was observed in pure iron (Gatelier-Roth ea *et al.*, 1992). The presence of 0.013 wt. % carbon in the form of intergranular carbides reduced the peak height and increased the width. If the carbon was instead present in solution, the height decreased and the width increased further. This was attributed to the retarding force of interstitial carbon on domain walls.

On intragranular precipitation of  $\epsilon$ -carbide from a solid solution, the BN maximum amplitude increased monotonically until precipitation was complete. When  $\text{Fe}_3\text{C}$  was instead precipitated, the amplitude increased at short ageing times, then subsequently decreased after precipitation was complete and coalescence of precipitates began to occur. At the longest times, the amplitude was approximately constant (Gatelier-Roth ea *et al.*, 1992). The variations were smaller from  $\epsilon$ -carbide than from cementite, because  $\epsilon$  is smaller, and no closure domains are generated; instead, the wall is bent by the precipitates. The areas under the peaks followed similar trends to the maximum amplitudes (Gatelier-Roth ea *et al.*, 1998). Intragranular precipitates affected BN behaviour more strongly than coarser, intergranular precipitates at the same carbon content.

In ferritic/pearlitic steels, the carbon content determines the proportion of the two components. The pulse height distribution extended to larger pulse sizes when the carbon content was greater (Clapham *et al.*, 1991). If individual domain wall displacement distances follow this distribution, this suggests that they are both larger and more varied in pearlite. However, another possible explanation is that the large event sizes are caused by many domain walls jumping together in an avalanche effect (§ 3.3.5).

Increasing the pearlite fraction decreased the MAE amplitude at  $H = 0$  and changed the form of the RMS BN versus  $H$  plot from two peaks to only one (Lo and Scruby, 1999). This behaviour was attributed to a larger proportion of Type-I walls when the pearlite content was lower. Conflicting results were obtained by Ng *et al.* (2001); a single sharp peak occurring at a negative  $H$  in a ferrite-cementite sample broadened and extended to both

sides of  $H = 0$  as the pearlite content was increased. Saquet *et al.* (1999) observed that the signal from ferrite-pearlite appeared to be a combination of the signals from the two components (Figure 4.12). However, the ratio of the heights of the two components of the curve is not the same as the volume ratio of ferrite to pearlite. The reasons suggested for this were the differences in carbon content in the two phases, or variations in correlation (avalanche) phenomena.

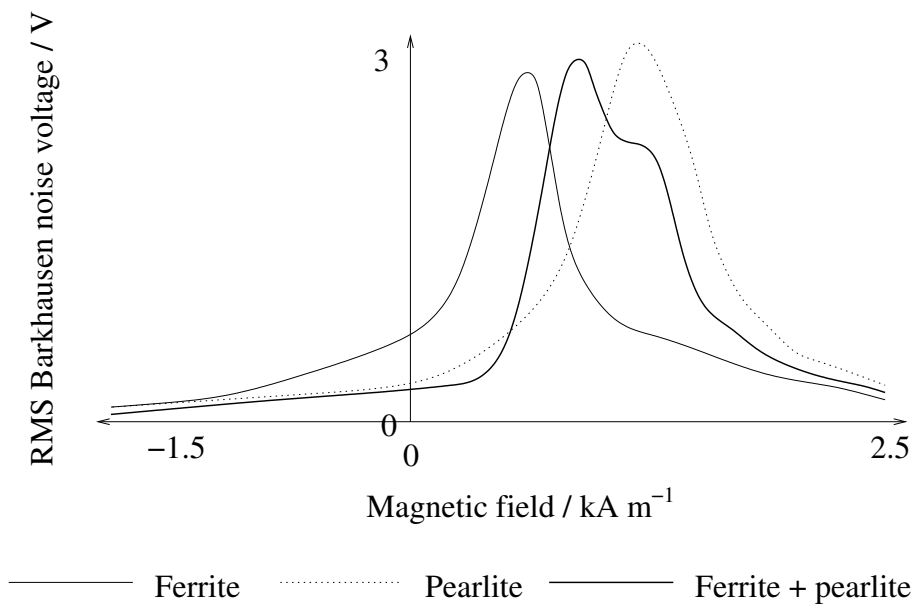


Figure 4.12: BN signals from ferritic, pearlitic and ferrite + pearlite microstructures in plain-carbon steel, showing two-component signal from the microstructure with two constituents (Saquet *et al.*, 1999).

#### 4.6.4 Summary

Coherent or regularly spaced particles give higher  $H_C$  and  $W_H$  than spheroidal particles at the same bulk composition, whether or not the particles are ferromagnetic. In plain-carbon steels,  $H_C$  increases monotonically with carbon content, but this may be modified by the presence of other elements. In alloys containing particles,  $H_C$  shows a clear correlation with hardness, whatever the particle morphology and composition.

Carbon in solution is believed to exert a drag force on domain walls. Small intragranular particles bend the domain walls, which move in a quasi-continuous manner, with parts of the wall moving a short distance in an individual event. On coarsening, the motion transforms into large, discrete jumps. The formation of closure domains after prolonged coarsening, and their interaction to form a domain network, is thought to limit the jump size. In steels with only a small carbon content, particle coarsening reduces  $H_C$  and the BN amplitude because of the decreased number density of pinning sites.

Particles appear to outweigh grain boundaries in their influence on magnetic properties. However, the presence of grain boundaries limits the maximum domain wall jump size.

Experiments on the effect of carbide morphology on BN yielded inconsistent results. In one study, increasing the fraction of pearlite in a ferrite-pearlite steel caused a transformation from double- to single-peak behaviour. In another, an initial single peak was found to broaden. The reasons for this discrepancy are not clear. A third investigation showed that the two-component microstructure produced a peak which appeared to be a simple combination of the peak shapes of the constituents. This is an important result since it suggests that parts of the BN signal can be related rather straightforwardly to individual microstructural components.

## 4.7 Magnetic properties of tempered steels

### 4.7.1 Changes in hysteresis properties on tempering

#### Plain-carbon steels

The hardness and  $H_C$  of a plain-carbon steel at different stages of tempering are shown in Figure 4.13 (Kameda and Ranjan, 1987a). The hardness decreased smoothly with increasing temperature, but  $H_C$  changed most dramatically between 200 and 400°C. This corresponds to the precipitation of  $\epsilon$ -carbide followed by fine needlelike  $\text{Fe}_3\text{C}$ .  $W_H$  followed the same dependence on temperature as  $H_C$ .

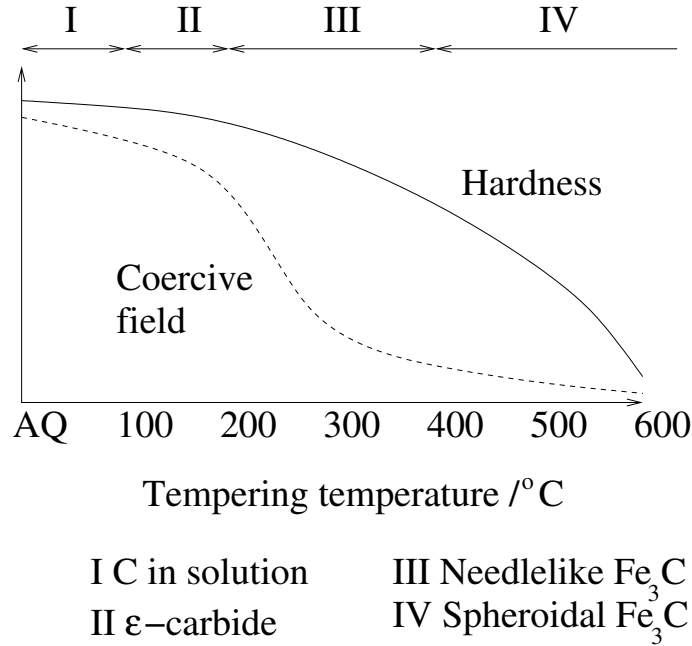


Figure 4.13: Changes in hardness and coercive field associated with different tempering times (Kameda and Ranjan, 1987a).

Under similar experimental conditions, Buttle *et al.* (1987c) observed a  $H_C$  curve shaped like the hardness curve in Figure 4.13, and a hardness curve similar to the  $H_C$  curve observed by Kameda and Ranjan. The difference in carbon content (0.17 wt. % for Kameda and Ranjan; 0.45–0.55 wt. % for Buttle *et al.*) could be responsible.

The hardness of a plain-carbon steel fell rapidly over the first hour of tempering at 600°C, then decreased more gradually at longer times (Moorthy *et al.*, 1998).  $H_C$ , after an initial decrease, peaked at 10 hours before decreasing smoothly. Peaks in  $B_R$  and the maximum induction  $B_{max}$  also occurred at this time, as did the onset of BN peak-splitting (§ 4.7.3).

Relationships between  $H_C$  and particle diameter  $\bar{d}_p$  were presented by Kneller (1962) and Mager (1962):

$$H_C \sim \bar{d}_p^{3/2} \quad (4.4)$$

for  $\bar{d}_p < \delta$ , where  $\delta$  is the domain wall thickness, and

$$H_C \sim \bar{d}_p^{-1/2} \quad (4.5)$$

for  $\bar{d}_p > \delta$ .

A maximum was therefore expected at an intermediate time in plots of  $H_C$  against tempering time (Hildebrand, 1997). Instead, two peaks were seen in both plain-carbon and alloy steels. A greater tempering temperature caused accelerated kinetics, and increasing the carbon content gave higher  $H_C$  values. The first peak was attributed to the appearance on martensite packet boundaries of needlelike carbides and their spheroidisation and coarsening, and the second to precipitation and coarsening of spheroidal particles in the interior of the former packets. Given the timescale of the first peak ( $\sim 10$  minutes at  $650^\circ\text{C}$ ), the carbides involved may well be  $\epsilon$ , rather than  $\text{Fe}_3\text{C}$  as stated by Hildebrand. The second peak occurs at around 100 minutes and is more prominent the greater the carbon content. Further peak structures could be seen in a sample containing chromium, but it appears that the effects of different carbides often overlap, since the effects of  $\text{MC}$  and  $\text{M}_6\text{C}$  could not be separated.

### Alloy steels

In 11Cr1Mo steel,  $H_C$ ,  $B_R$ ,  $W_H$  and hardness decreased rapidly with tempering time for periods up to 100 s (Yi *et al.*, 1994). Above this, the decrease became more gradual.  $B_S$  increased with tempering time, also with a slope change from rapid to gradual at 100 s. A monotonic decrease in  $H_C$  with increasing hardness was observed.

A secondary hardening peak was seen for  $2\frac{1}{4}\text{Cr1Mo}$  and  $9\text{Cr1Mo}$  steels tempered at  $650^\circ\text{C}$ , and  $H_C$  also decreased rapidly, peaked at an intermediate time, then decreased gradually (Moorthy *et al.*, 1998, 2000).

The discrepancies between these results and those of Yi *et al.*, in which a secondary peak might also have been expected, may be reconciled by considering the wide range of timescales on which the  $H_C$  peaks were observed by Hildebrand (1997). In the lower-chromium steels, the second ‘Hildebrand’ peak may occur at a longer time than in the 11Cr1Mo sample so that it is

visible in  $2\frac{1}{4}\text{Cr1Mo}$  and  $9\text{Cr1Mo}$  but occurs before the first measurement in  $11\text{Cr1Mo}$ .

## 4.7.2 Effect of tempering on magnetic noise

### Bulk noise properties

Quenched and tempered samples of 0.4C-5Cr-Mo-V steel were prepared with a range of prior austenite grain sizes and carbide sizes (Nakai *et al.*, 1989). The BN power increased linearly with the mean carbide diameter, and decreased with increasing number of carbide particles per unit area. There was a trend towards smaller BN power values as the prior austenite grain size increased but the correlation was less clear than those for the carbides.

### Noise peak shapes

Kameda and Ranjan (1987a) observed an MAE peak at each of the hysteresis loop knees, but only a single BN peak. On decreasing the field from positive to negative, the largest MAE pulses occurred at the negative knee. This peak increased in height with tempering temperature; the greatest change occurred between 200 and 500°C. This range corresponds to the precipitation of fine  $\epsilon$  and  $\text{Fe}_3\text{C}$ , and the beginning of  $\text{Fe}_3\text{C}$  spheroidisation. The position of this peak remained constant, but both the positive MAE peak and the BN peak moved further from  $H = 0$  with increasing temperature. The BN peak height increased with tempering temperature in three distinct stages, corresponding to solid solution, precipitation of  $\epsilon$ -carbon and needlelike  $\text{Fe}_3\text{C}$ , and spheroidisation of  $\text{Fe}_3\text{C}$ .

Analysis of the RMS noise signal revealed changes in the BN peak shape and a split into two peaks after high-temperature tempering (Figure 4.14; Buttle *et al.*, 1987c). The single, asymmetric peak from the as-quenched material increased in height with increasing temperature. A discernible ‘shoulder’ appeared at 500°C, and this grew into a second peak of similar height to the first. Broadening of the signal to a greater range of fields was also observed. The initial single BN peak was attributed to the martensitic structure, and the second to the precipitation of cementite at 500°C.

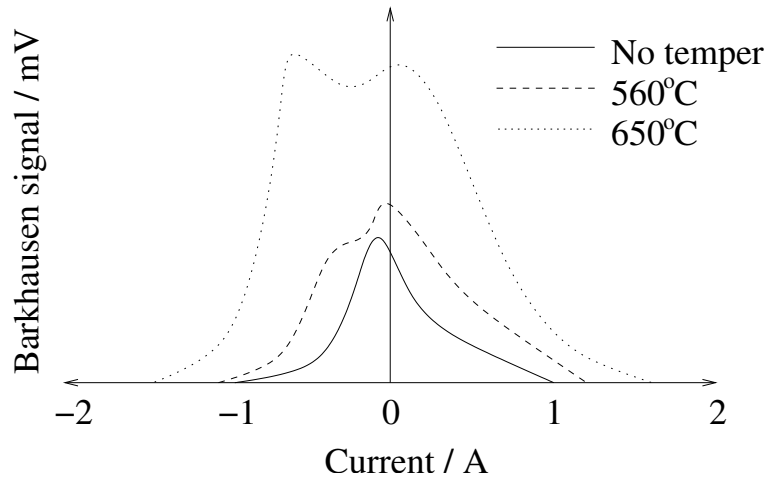


Figure 4.14: Changes in BN peak size and shape due to tempering (Buttle *et al.*, 1987c).

No observable MAE activity occurred at or below 350°C. This was attributed to the tetragonality of martensite, which favoured Type-II walls because of the unique easy axis. As the martensite relaxed to ferrite, this constraint was removed, and Type-I activity and hence MAE could occur. Two peaks appeared, one on either side of  $H = 0$ . These were larger the higher the tempering temperature. The initial peak, on the negative side of  $H = 0$ , was always the larger.

Figure 4.15 shows the change in RMS BN peak shape with tempering temperature observed in a very similar experiment (Saquet *et al.*, 1999). The peaks were narrower and higher, and occurred at smaller  $H$ , when the temperature was higher. This was accompanied by a change in the hysteresis loop shape, from broad and sheared to narrower, with straighter sides and a higher  $M_S$ . Single peaks were observed in MAE signals, at the same positions as the BN peaks; both occurred close to  $H_C$  as determined from the hysteresis loops.

In as-quenched steel, the noise was of a higher frequency ( $\sim 100$  kHz) than in the tempered samples ( $\sim 10$  kHz). The small amplitude of peaks from as-quenched steel was attributed to the greater attenuation by eddy currents of higher-frequency noise. This reduces the proportion of noise reaching the

pickup coil. Since the degree of attenuation, and the frequency filtering, may vary from one set of experimental apparatus to another, this could explain some of the discrepancies between the results of Saquet *et al.* and those of Buttle *et al.* (1987c).

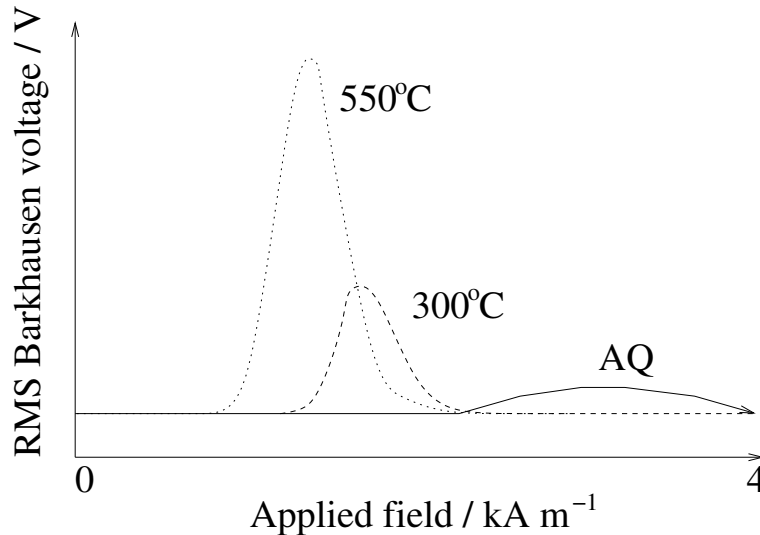


Figure 4.15: Change in the shape of the BN signal from as-quenched (AQ) state due to tempering for one hour at 300 and 550°C (Saquet *et al.*, 1999).

### 4.7.3 Changes in BN with tempering time

Samples of a plain-carbon steel were tempered at 600°C for times ranging from 0.5 to 100 hours (Moorthy *et al.*, 1997b). The average carbide size increased from 0.13  $\mu\text{m}$  after 1 hour of tempering, to 0.46  $\mu\text{m}$  after 100 hours. The carbide size distribution also broadened approximately four-fold. Equiaxed ferrite replaced the original martensitic structure, and coarsened as tempering progressed.

The as-quenched BN peak occurred at  $H = 4 \text{ kA m}^{-1}$ , which is comparable with the value of 2.5–3  $\text{kA m}^{-1}$  observed by Saquet *et al.*, given the difference in composition. Tempering for 0.5 hours shifted the peak to a smaller field and greatly increased its amplitude. This change was attributed to the increase in domain wall mobility and mean free path as the dislocation

density decreased. After 1 hour, the peak broadened and showed a change in slope, which developed into a second distinct peak, clearly visible after 5 hours (Figure 4.16). Further tempering increased the separation of the peaks and reduced the signal amplitude. The peak shapes were different from those observed by Saquet *et al.* after 1 hour of tempering at 550°C; in particular, the onset of noise activity occurred before  $H = 0$  in the observations of Moorthy *et al.*, but well past  $H = 0$  in those of Saquet *et al.*.

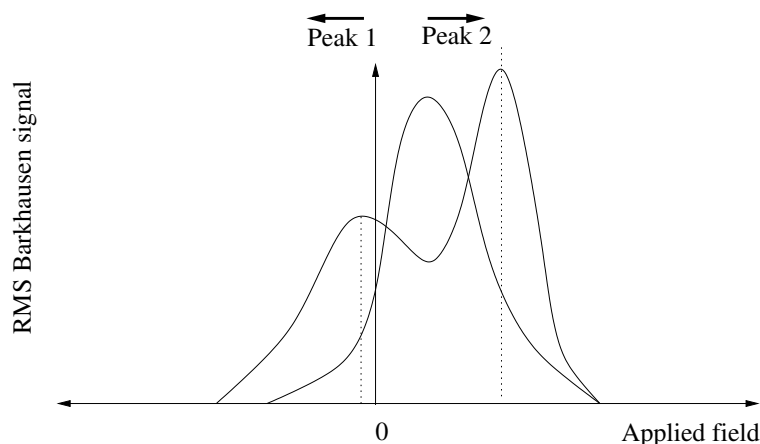


Figure 4.16: Development of two-peak behaviour with increasing tempering time (Moorthy *et al.*, 1997b).

The peak-splitting was explained as follows: the BN was due mainly to domain wall motion pinned by carbide particles and grain boundaries, rather than to domain nucleation or annihilation. (It was considered that, since ideal saturation was difficult to achieve in practice, domain nucleation would not be likely since domains had not previously been annihilated. Dislocations were believed to exert a general retarding effect rather than participating in pinning.) The transformation of martensite to ferrite and carbides creates two distributions of domain wall pinning sites due respectively to grain boundaries and precipitates. Prolonged tempering causes coarsening of both carbides and grains. This increases the magnetostatic energy associated with each particle (§ 3.3.1) but reduces the energy of grain boundaries by annihilating boundary dislocations. Carbides therefore become stronger pinning

sites as grain boundaries become weaker. Peak 1, at the lower applied field, is due to grain boundary pinning, and Peak 2 to carbides.

Both types of sites were characterised as distributions of critical pinning fields  $H_{\text{crit}}$  with average critical pinning fields  $\bar{H}_{\text{crit}}$  and ranges  $\Delta H_{\text{crit}}$  characterising the width. At short tempering times, the  $\bar{H}_{\text{crit}}$  values for the two distributions were similar and the ranges overlapped, giving a single peak. After a longer time, the distinct distributions could clearly be seen.

The position of Peak 1 on the  $H$  axis gave a good linear correlation with the average grain size (Moorthy *et al.*, 1998; Figure 4.17) and that of Peak 2 was even more clearly related to the average carbide size (Figure 4.18). This lends support to the suggested interpretation.

Peak heights were attributed to a combination of the number of domain wall events and the mean free path of walls. The Peak 1 height initially increased; this was explained by the coalescence of laths increasing the mean free path. Its subsequent decrease was attributed to the reduction in the number of domain walls as grains or laths coarsened. The height of Peak 2 was observed to be greatest for a narrow size distribution of carbides, and least when the distribution became broader on longer tempering.

Very similar peak-splitting was observed in  $2\frac{1}{4}\text{Cr1Mo}$  and  $9\text{Cr1Mo}$  steels, but with delayed kinetics; an obvious double peak was only seen after 50 hours of tempering at  $650^\circ\text{C}$ , as opposed to 5 hours at  $600^\circ\text{C}$  in the plain-carbon steel (Moorthy *et al.*, 1998, 2000).

The height of Peak 1 dropped rapidly after 500 hours' tempering in the  $2\frac{1}{4}\text{Cr1Mo}$  steel, and after 200 hours in  $9\text{Cr1Mo}$ . This was explained by the dissolution of fine, needlelike  $\text{M}_2\text{X}$  particles. These are too small to be efficient pinning sites in their own right, but their presence retards grain and lath coarsening and dislocation annihilation. On dissolution, grain sizes increase rapidly, giving a marked reduction in the number of domains, and hence in the peak height. Moorthy *et al.* suggested, on the basis of work by Goodenough (1954), that needles or plates of  $\text{M}_2\text{X}$  acted as domain nucleation sites, whereas spheroidal carbides such as  $\text{M}_7\text{C}_3$  and  $\text{M}_{23}\text{C}_6$  did not. Decreases in Peak 2 height were linked with the dissolution of  $\text{M}_2\text{X}$  and precipitation of spheroidal carbides. Since their diameter ( $\sim 0.5 \mu\text{m}$ ) is greater

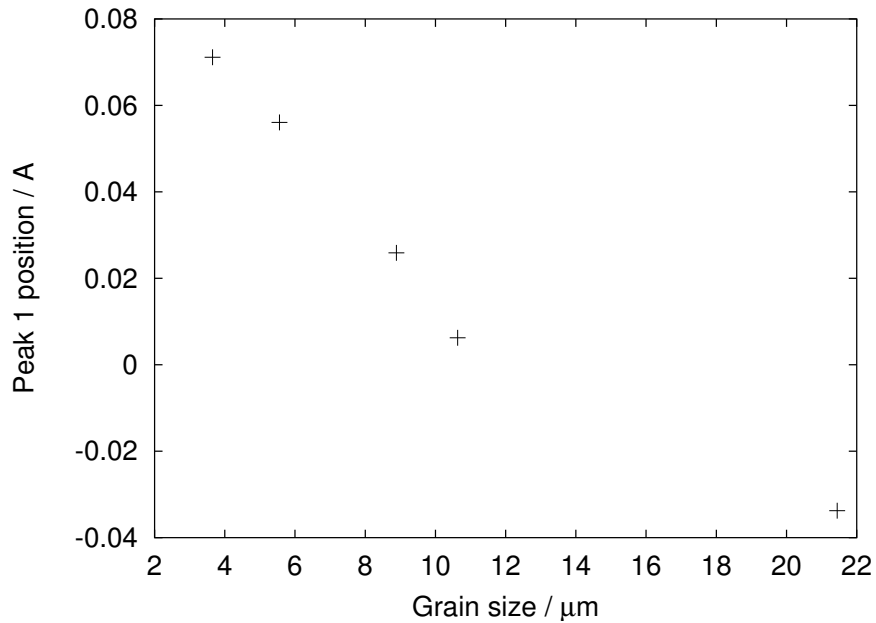


Figure 4.17: Relationship between Peak 1 applied field and grain size (Moorthy *et al.*, 1998).

than the critical value for spike domain formation ( $0.2 \mu\text{m}$ ), it is likely that large carbides have associated spikes. Longer-range interaction is possible between domain walls and spikes than between walls and particles alone, giving a smaller domain wall mean free path.

11Cr1Mo steel was tempered at  $650^\circ$  for a range of times between 10 minutes and 80 hours, and the total number of BN counts and BN energy (defined as the integral of the square of the BN amplitude over one magnetisation cycle) were measured (Yi *et al.*, 1994). Both quantities displayed the same dependence on tempering time. An initial increase was followed by a plateau, a second more gradual increase, and a further plateau.

Based on microscopic observations, the initial increase was attributed to the precipitation of carbides from solid solution, releasing internal stresses, during the first hour of tempering. It was noted that noise pulses were large and tended to cluster together, with the jumping of one domain wall inducing the movement of a neighbour. The gradual increase in noise energy

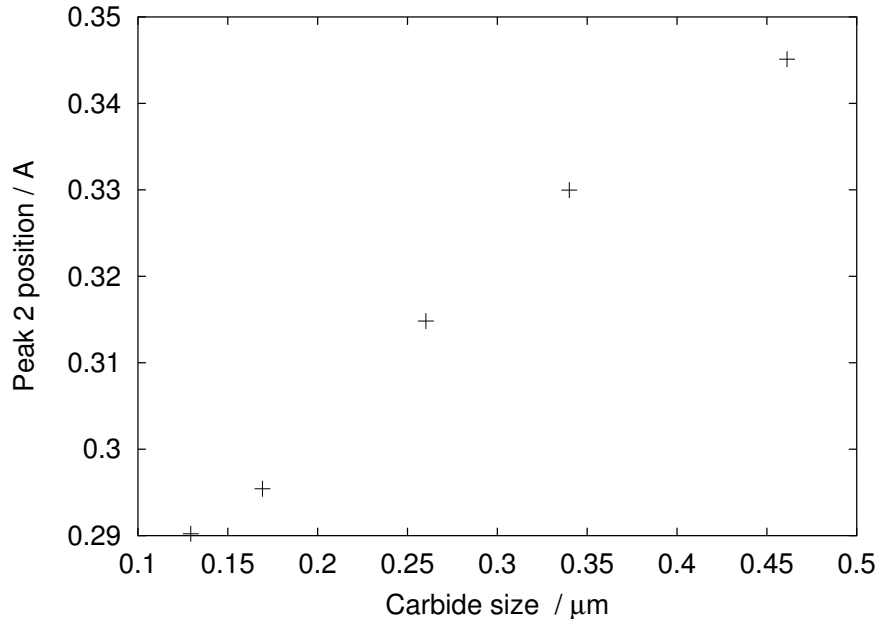


Figure 4.18: Relationship between Peak 2 applied field and carbide size (Moorthy *et al.*, 1998).

between 1 and 20 hours was attributed to the coarsening and reduction in number density of  $\text{M}_{23}\text{C}_6$  particles; this increases the interparticle distance and hence the size of individual Barkhausen events. In the final stage, the observed abrupt change in noise energy was found to occur concurrently with a rapid decrease in dislocation density.

The measurements were made using a small range of applied field, such that only pinned domain wall motion should occur and nucleation and annihilation should be avoided. Within this regime, both the BN energy and the number of counts were linearly related to the hardness.

#### 4.7.4 Summary

The most pronounced change in  $H_C$  on tempering in plain-carbon steel was associated with the precipitation of needlelike carbides from solution. During prolonged tempering at 600–650°C, maxima in hardness and  $H_C$  appeared in some cases but not in others. Measurements of  $H_C$  at very short tem-

pering times revealed two distinct peaks, the first of which occurred within  $\sim 10$  minutes of the start of tempering. The timescale of the second varied; this may be the reason for the discrepancies seen in other studies. The simple relationships between  $H_C$  and hardness observed in other materials do not always hold in tempered steels.

In as-quenched samples, little or no MAE activity was seen, but peaks appeared at the ‘knees’ of the hysteresis curve after tempering, and grew in height with increasing tempering temperature. Although the precise characteristics of the BN peak shapes vary considerably from one experimental study to another, there is a trend towards higher peaks at lower  $H$ , signifying weaker pinning, with increasing tempering temperature. Prolonged, high-temperature tempering causes the peak to split into two parts, which separate and decrease in height with tempering time. Moorthy *et al.* (1997b, 1998, 2000) explained the peak shapes in terms of distributions of pinning sites from carbides and grain boundaries, and supported the interpretation with linear relationships between peak positions and microstructural feature dimensions.

## 4.8 Are the results inconsistent?

Concerns have been raised over discrepancies between magnetic noise results, for example variations in the number and shape of BN peaks in different studies on very similar materials (Moorthy *et al.*, 1997b; Saquet *et al.*, 1999, Sablik and Augustyniak, 1999). It has been suggested that inconsistencies in experimental apparatus and conditions are the cause.

It is true that conditions vary widely. As an illustration, Table 4.2 demonstrates the differences in applied field range, frequency and filtering used in experiments on tempered steels. It has been shown that changes in these parameters can alter the BN characteristics (§ 4.9.3, § 4.9.4) and even the number of peaks (Kim *et al.*, 1992). However, taking this into account, some conclusions can still be drawn (§ 4.10).

	Waveform	Frequency / Hz	Field range /kAm <sup>-1</sup>	Filtering range / kHz
Kameda & R., 1987a	?	varied	±14.3	1–300
Buttle <i>et al.</i> , 1987c	triangular	$5 \times 10^{-3}$	±21.6	$3 \times 10^{-4}$ –0.36
Saquet <i>et al.</i> , 1999	triangular	0.1 Hz	±20	0.5–500
Moorthy <i>et al.</i> , 1998	triangular	0.1 Hz	±12	0.1–100
Nakai <i>et al.</i> , 1989	triangular	1 Hz	?	10–700
Yi <i>et al.</i> , 1994	sine	0.1 Hz	±2.4	1–150

Table 4.2: Experimental conditions used in BN and MAE measurements on tempered steels.

## 4.9 Effects of magnetising parameters

### 4.9.1 Surface condition

Because of attenuation by eddy currents, the penetration depth of the BN excitation field is small ( $\sim 0.1$  mm) and measurements may therefore be strongly influenced by surface condition, particularly strain.

Coarse grinding and fine polishing did not produce any noticeable difference in the BN signals of plain-carbon steel samples (Clapham *et al.*, 1991). However, in nickel, the influence of surface finish was pronounced, especially when the rate of change of field with time was high (Hill *et al.*, 1991). Vigorous grinding of steel, at feed rates up to  $12.7 \mu\text{m s}^{-1}$ , caused changes in the measured RMS Barkhausen voltage compared to the signal measured at low feed rates (Parakka *et al.*, 1997). At such high rates, transformation to austenite can occur, leading to the formation of a martensitic layer when the surface is quenched with coolant.

Yoshino *et al.* (1996) found that the importance of the surface condition on  $H_C$  measurements depended on the magnetising frequency. The surface finish and the degree of oxidation were found to have little effect when magnetisation took place at a very low frequency (0.005 Hz), but to increase the measured  $H_C$  when a higher frequency (0.1 Hz) was used.

### 4.9.2 Magnetising field waveform

A number of different waveforms have been used for the alternating excitation field to obtain BN signals. The most common of these are triangular and sinusoidal, but square waves are also occasionally used. Sipahi *et al.* (1993) found that the noise frequency content was similar when obtained with the triangular or sinusoidal waveform, but was significantly altered by using a square wave. Square waves were more likely to introduce spurious data than either sinusoidal or triangular waves. It was therefore considered that sinusoidal or triangular waveforms should be preferred for BN studies.

### 4.9.3 Magnetising frequency

In a plain-carbon steel, the RMS BN voltage was higher, and larger peaks were observed, at higher magnetising frequencies (Dhar and Atherton, 1992). This result was true for a variety of applied field amplitudes. The suggested reason was that a greater number of domain walls participated in magnetisation at higher frequencies. However, it was admitted that the precise effect of frequency was difficult to determine.

Similarly, the maximum amplitude of both BN and MAE increased with frequency in a quenched and tempered plain-carbon steel (Kameda and Ranjan, 1987a).

In MAE, the integrated signal was found to be linearly related to magnetising frequency at higher frequencies, but to deviate from linearity at lower values, in both mild steel and nickel (Ng *et al.*, 1996). A model was suggested to explain this behaviour: the observed signal was attributed to a component from domain wall motion and a component from nucleation and annihilation. The different dependences of these on frequency were used to account for the shape of the curve.

A wide variety of magnetising frequency settings are found in the literature (*e.g.* Table 4.2). Work by Moorthy *et al.* (2001) has demonstrated, in addition, that variations in both the frequency and the filtering range can significantly affect the shape of a BN voltage peak, and even the number of peaks visible. It would therefore be advisable to introduce more consistency

into experimental design to ensure repeatability.

#### 4.9.4 Magnetising field amplitude

It has been seen that modification of  $H_{\max}$  can affect the number of BN peaks observed (Kim *et al.*, 1992; § 4.5.3).

In a plain-carbon steel, the RMS BN voltage increased smoothly to a maximum at an intermediate  $H_{\max}$  value, then decreased at higher  $H_{\max}$  (Dhar and Atherton, 1992). The increase was attributed to the greater capacity for overcoming pinning obstacles when the applied field was larger, and the decrease to the predominance of domain rotation over domain wall motion at very high fields. The same form of dependence of RMS voltage on  $H_{\max}$  was seen for all frequencies investigated.

The dependence of RMS BN voltage on  $H_{\max}$  is shown in Figure 4.19 for three microstructures with the same composition: bainitic, pearlitic and spheroidised pearlite (Mitra *et al.*, 1995). There is clearly a complex interdependence between magnetising frequency,  $H_{\max}$  and microstructural state, and this may account for the discrepancies seen in BN results. It would be useful to conduct a systematic investigation of the dependence of peak shapes, RMS voltages, *etc.* for a wide range of compositions and microstructures to give a deeper understanding of these issues.

#### 4.9.5 Demagnetising and stray fields

The demagnetising effect (§ 3.1.3) reduces the actual field experienced when a given field is applied.  $H_C$  should be independent of the demagnetising field (Swartzendruber, 1992) but in practice can have some shape-dependence (Blamire, personal communication). Other properties, including BN and MAE characteristics, are subject to demagnetising fields.

Stray fields are those which result from incomplete magnetic circuits, for example at air gaps between a magnetic yoke and a sample surface. In MAE experiments, nonmagnetic spacers are customarily used between the yoke and the surface to minimise extraneous noise. However, these spacers introduce demagnetising and stray fields. Ng *et al.* (1994) found that varying the spacer

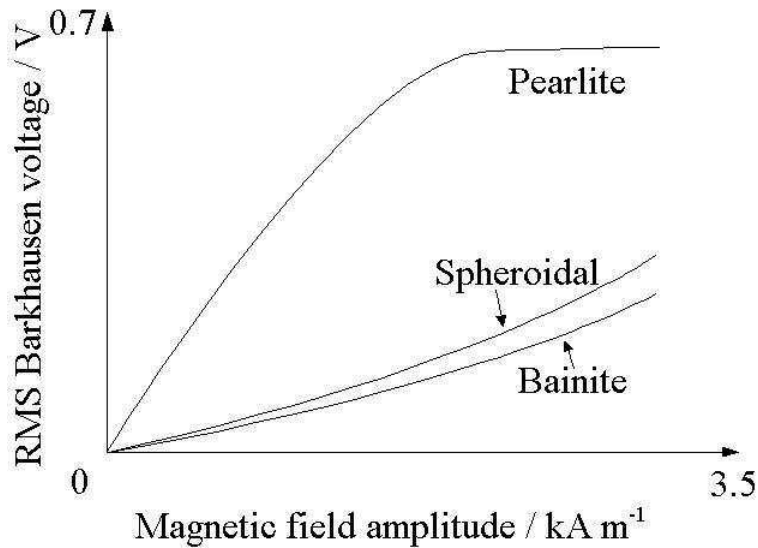


Figure 4.19: Dependence of the RMS BN voltage on applied field amplitude, after Mitra *et al.*, 1995

thickness caused significant changes to MAE peak shapes and even to the number of peaks observed. In nickel, increasing this thickness caused a single peak to split into three, and in mild steel the two peaks present moved apart and decreased in height. It is clear from these results that even small changes in the level of demagnetising or stray fields can have dramatic effects on the observed signal. This is another possible reason for observed discrepancies in results.

#### 4.9.6 Stress

The magnetic behaviour of steels is influenced significantly by elastic stresses via the magnetoelastic effect, such that the evaluation of stress states by magnetic techniques is a large research field.

The BN voltage was measured as a function of the angle between the applied field direction and the axial direction of a steel pipe (Jagadish *et al.*, 1990). An applied tensile stress changed the angle of maximum BN voltage. This observation has important consequences for in-situ microstructural monitoring in stressed components.

### 4.9.7 Temperature

The transition between ferromagnetic and paramagnetic behaviour at the Curie temperatures of certain carbides can produce an anomaly in the measured  $H_C$  (English, 1967). From the two examples given by English, it appears that  $T_C$  can vary by at least 200°C depending on composition. Anomalies could cause confusing results if the temperature during NDT is close to  $T_C$  for any of the carbides present. However, it may also be possible, after a systematic study, to make use of the phenomenon for identification of phases and monitoring of their compositions.

A further temperature effect is thermal activation, which allows domain walls to overcome pinning sites more easily (Pardavi-Horvath, 1999) but this does not seem to have been investigated extensively.

### 4.9.8 Magnetic history

On repetition of an earlier measurement on a steel pipe, it was found that the direction in which the greatest BN voltage was observed had changed by 30° (Jagadish *et al.*, 1990). It appeared that the repeated magnetisation and demagnetisation during experiments had altered the magnetic properties of the sample. This effect does not appear to have been documented elsewhere, but it may present difficulties for NDT applications.

### 4.9.9 Solute segregation

Segregation of solutes, although it did not affect the hysteresis properties, was detectable by both BN and MAE measurement (Kameda and Ranjan, 1987b). For constant carbide morphology and hardness, the RMS and maximum MAE voltages increased as a greater proportion of solute segregated to grain boundaries. The maximum BN voltage was a minimum for an intermediate level of segregation. The results were the same for Sn, Sb and P dopants; this means that magnetic noise is not useful for monitoring grain boundary embrittlement, the degree of which depends on the chemistry of the segregant.

## 4.10 Summary and conclusions

Magnetic hysteresis and noise properties have been investigated for use in microstructural testing. Clear relationships between  $H_C$  and microstructural feature sizes, carbon content or hardness have often been found in simple systems such as equiaxed ferrite. However, these do not always hold in more complicated microstructures such as tempered martensite.

BN and magnetoacoustic emission signals can be difficult to interpret, and the discrepancies in results are well documented. Nonetheless, general results have emerged from this review. Magnetically hard materials, containing strong pinning sites, tend to produce a single BN peak, which can be attributed to pinned wall motion. Fine structure is sometimes seen on this peak if microstructural constituents have sufficiently different pinning strengths. In softer materials, by contrast, two peaks positioned at the ‘knees’ of the hysteresis curve are present in addition to, or in place of, the single peak. These, because of their position, are believed to arise from domain nucleation and annihilation. Reducing the applied field range in these samples, so that the material is only cycled through a minor loop, suppresses the outer peaks. It is suggested that increasing the level of pinning has a similar effect, preventing domain nucleation and annihilation.

Single-value BN or MAE parameters such as the total number of counts or maximum noise amplitude can be related to microstructural data in simple systems, but may not always be useful when more than one microstructural feature is changing. Analyses of the entire signal contain more information and, in particular, allow the variation in pinning field strength to be followed.

Experimental conditions, such as the magnetising frequency and  $H_{\max}$ , can significantly affect the measured noise signals. Because of this, it would be advisable to adopt a standard set of experimental practices, or to conduct systematic studies of the effects of magnetising conditions on the material of interest before using magnetic methods for NDT.